Phys Chem Minerals (1998) 25:469–484

ORIGINAL PAPER

H. Taura · H. Yurimoto · K. Kurita · S. Sueno

Pressure dependence on partition coefficients for trace elements between olivine and the coexisting melts

Received: March 6, 1997 / Revised, accepted: March 12, 1998

Abstract Partition coefficients between olivine and melt at upper mantle conditions, 3 to 14 GPa, have been determined for 27 trace elements (Li, Be, B, Na, Mg, Al, Si, P, K, Ca, Sc, Ti, V, Cr, Mn, Fe, Co, Ni, Cu, Rb, Sr, Y, Zr, Cs, Ba, La and Ce) using secondary-ion mass-spectrometry (SIMS) and electron-probe microanalysis (EPMA). The general pattern of olivine/melt partitioning on Onuma diagrams resembles those reported previously for natural systems. This agreement strongly supports the argument that partitioning is under structural control of olivine even at high pressure. The partition coefficients for mono- and tri-valent cations show significant pressure dependence, both becoming larger with pressure, and are strongly correlated with coupled substitution into cation sites in the olivine structure. The dominant type of trace element substitution for mono- and tri-valent cations into olivine changes gradually from (Si, Mg)↔(Al, Cr) at low pressure to (Si, Mg)↔(Al, Al) and (Mg, Mg)↔(Na, Al) at high pressure. The change in substitution type results in an increase in partition coefficients of Al and Na with pressure. An inverse correlation between the partition coefficients for divalent cations and pressure has been observed, especially for Ni, Co and Fe. The order of decreasing rate of partition coefficient with pressure correlates to strength of crystal field effect of the cation. The pressure dependence of olivine/melt partitioning can be attributed to the compression of cation polyhedra induced by pressure and the compensation of electrostatic valence by cation substitution.

Hiroshi Taura[1] · Hisayoshi Yurimoto (✉)[2] · Kei Kurita[3]
Shigeho Sueno
Institute of Geoscience, University of Tsukuba, Tsukuba, Ibaraki 305 Japan

Present address:
[1] Foundation for Promotion of Material Science and Technology of Japan, Setagaya, Tokyo, Japan
[2] Department of Earth and Planetary Sciences, Laboratory for Planetary Sciences, Tokyo Institute of Technology, Meguro, Tokyo 152 Japan,
Fax: +81-3-5734-3538, e-mail: yuri@geo.titech.ac.jp
[3] Department of Geophysics, University of Tokyo, Hongo, Tokyo, Japan

Introduction

It is believed that a magma ocean existed at the beginning of Earth's history (e.g. Abe 1993). Minerals crystallized from the magma ocean would have had different compositions from the host magma, and it has been suggested that gravitational separation of minerals from liquid in the magma ocean played an important role in the formation of a layered mantle structure (Herzberg 1984; Ohtani 1984; Agee 1993). Deviations in element partitioning from unity between minerals and coexisting melt leads to compositional evolution in the melt upon crystal segregation, creating a heterogeneous distribution of elements in the mantle. This segregation would control the spatial distribution of elements in the Earth's interior. In particular, olivine is a major constituent in the mantle and is the liquidus mineral in peridotitic mantle to depths of about 400 km (Takahashi 1986; Zhang and Herzberg 1994). Therefore, a knowledge of the pressure dependence on elemental partitioning between olivine and magma is important for understanding mantle structure, chemical evolution, and magma generation.

Many high-pressure experiments have been carried out on model mantle compositions (Ohtani et al. 1986; Scarfe and Takahashi 1986; Takahashi 1986; Zhang and Herzberg 1994). However, studies for element partitioning between olivine and melt under mantle conditions are limited. Dependence of element partitioning on composition, temperature and pressure between olivine and the coexisting melts has been studied for many divalent cations such as Ni, Mg, Co, Fe, Mn and Ca (Takahashi 1978; Jurewicz and Watson 1988). Recently, the partitioning of trivalent cations have also reported (Colson et al. 1988; Agee and Walker 1990; Beattie 1994; Suzuki and Akaogi 1995). Agee and Walker (1990) reported that the partition coefficient of Al between olivine and silicate liquid, $D_{Al}^{ol/melt}$, increases with pressure up to 6 GPa. Ozawa (1991) confirmed the results of Agee and Walker and showed that $D_{Na}^{ol/melt}$ also increased with pressure up to 14.4 GPa, whereas, $D_{Cr}^{ol/melt}$ decreases with pressure. On the basis of these results, Ozawa suggested that there is a relatively large pressure depen-

dence on elemental partitioning of monovalent and trivalent cations between olivine and melt.

In this study, we have measured trace element abundances in olivine and coexisting melt in high-pressure melting experiments by secondary-ion mass-spectrometry (SIMS) and electron-probe microanalysis (EPMA). This paper focuses on the systematics of cation partitioning between olivine and melt at high pressure.

Experimental

High-pressure experiments were carried out using the MA-8 type apparatus at the Earthquake Research Institute, University of Tokyo. All runs were made using the quenching method. The starting material was natural peridotite powder KLB-1 (Takahashi 1986), which was pre-heated in Ar at 1273 K for an hour before experiments to assure anhydrous conditions. Run pressures ranged from

Table 1 Run conditions of high pressure experiments (*ol* olivine, *l* liquid, *C* carbon, *Re* rhenium)[a]

Run Name	Temperature/K	Pressure/GPa	Duration/min	Phase	Capsule
KLB-13	2173	7	25	ol+l	C
KLB-15	2173	5	20	ol+l	C
KLB-17	2073	5	60	ol+l	C
KLB-20	2173	5	30	ol+l	C
KLB-22	1873	3	40	ol+l	C
KLB-23	1973	5	60	ol+l	C
KLB-25	2073	7	60	ol+l	C
KLB-28	2073	3	60	ol+l	C
KLB-31	2273	9.7	10	ol+l	Re
KLB-35	2073	9.7	10	ol+l	Re
KLB-43	2173	14.4	5	ol+l	Re

[a] All run products are the same as those of Ozawa (1991).

Table 2 Measurement masses, typical sensitivity factors of SIMS analysis and element abundances of reference standards

Element	Mass number	Sensitivity factor	JB-1a[a] (ppm)	JR-1[a] (ppm)	San Carlos olivine[b] (ppm)
Li	7	0.24	11.5	62.3	1.3[c]
Be	9	0.18	1.4	3.1	
B	11	1.15	12.4	133	0.4[c]
Na	23	1.16	20300	30400	2.6[c]
Mg	26	0.42	46700	543	308200
Al	27	0.49	76800	68200	11[c]
Si	30	–	243900	352600	194600
P	31	6.74[d]	1130	87	39[c]
K	39	2.12	11800	36600	0.5[c]
Ca	40	0.50	66000	4500	84[c]
Sc	45	0.49[d]	29	5.2	3.1[c]
Ti	47	0.80	7790	559	5.9[c]
V	51	1.28	220	<8	4.8[c]
Cr	52	1.19	415	2.3	107[c]
Mn	55	1.54	1160	775	775
Fe	56	2.12	63600	6690	55700
Co	59	2.78	39.5	0.65	85[c]
Ni	60	4.68[e]	140	0.66	2900
Cu	63	5.21	55.5	1.4	0.5[c]
Rb	85	5.54	41	257	
Sr	88	1.56	443	30	0.3[c]
Y	89	1.34	25	46	
Zr	90	1.79	144	102	0.1[c]
Cs	133	8.70–18.78[f]	1.2	20.2	
Ba	138	3.61	497	40	
La	139	2.51	38	21	
Ce	140	2.68	67	49	

[a] Recommended value of Ando et al. (1989).
[b] Determined by EPMA analysis.
[c] Determined by SIMS analysis using JB-1a glass standard.
[d] ^{31}P and ^{45}Sc were interfered by SiH and SiO, AlO, respectively, The interferences were removed using JB-1a and JR-1 glass standards by the method of Yurimoto et al. (1989).
[e] Determined by the olivine standard. ^{60}Ni ions were interfered by $^{44}Ca^{16}O^{+}$ molecular ions for Ca rich materials (Yurimoto et al. 1991). The interference of $^{44}Ca^{16}O^{+}$ molecular ions could be removed by sensitivity factor of Ni of San Carlos olivine. The CaO interference percentage of secondary ion intensities for mass 60 were 0.15–0.55% and 5–25% for olivine and melt phases of run products, respectively.
[f] Sensitivity factor of Cs was dispersed because of low concentration in JB-1a glass, so that the concentration might not be determined precisely.

3 to 14.4 GPa. Tungsten carbide cubic anvils having 12-mm corner truncation edges were used in the range from 3 to 7 GPa, and anvils with 8-mm and 4-mm truncations were used from 7 to 12 GPa and from 12 to 14.4 GPa, respectively. Carbon capsules were used below 7 GPa, and rhenium capsules were used above 7 GPa because of carbon-diamond transformation. Cylindrical carbon heaters were used below 7 GPa, and $LaCrO_3$ heaters were used above 7 GPa. W3%Re-W25%Re thermocouples were used to measure sample temperature and chromel-alumel thermocouples were used to measure the temperature of the anvil surface. The temperature values were not corrected for the effect of pressure on EMF. Run durations were from five to sixty minutes. All of the run charges are the same as those described in Ozawa (1991), and further details on the experiments are described therein. Run conditions are listed in Table 1.

Recovered charges were prepared as polished thin sections to observe and to analyze coexisting phases. Solid and quenched liquid phases were distinguished using textural criteria as observed with the optical microscope and back-scattered electron image (BEI). Major elemental compositions of each phase were analyzed by EPMA (JEOL-JXA8621) at the Chemical Analysis Center, University of Tsukuba. The analytical conditions were a 20 kV accelerating voltage, a probe current of 10 nA, and X-ray accumulation time was 10 s for each element. The beam spot of about 10 μm in diameter was used to measure phenocryst crystals, whereas a 50 μm beam size was used for the quenched melt phase. Since the quench crystals are less than μm size, the beam was large enough to measure adequately the mean composition of the liquid phase. Line analyses across olivine/melt boundaries were done to evaluate equilibrium between olivine and melt. Beam diameters of 3 μm and 5 μm were used to evaluate chemical heterogeneity of olivine and melt phases, respectively.

Following the EPMA analysis, 27 trace elements were determined in each phase by SIMS (modified CAMECA ims-3f[1]) at the University of Tsukuba. Samples were coated with gold film (30 nm) in order to eliminate electrostatic charge build-up on the surface during analysis. The primary ion beam was composed of negatively charged monovalent oxygen ($^{16}O^-$) ions which were generated by a duoplasmatron. The primary high voltage was set to about −10 kV. The primary beam was focused on the sample surface with a diameter of 10–25 μm, and the primary beam current ranged from 2 to 8 nA. The secondary high voltage was +4.5 kV and the offset voltage was set to −100 V, while the energy slit was adjusted to 20 eV in order to remove molecular ion interferences. The mass resolution was set to ∼300. Measurements were made by cycling through mass sequences in a peak jumping mode. Secondary ion signals were detected with an electron multiplier. Standards used for quantitative analysis were JB-1a and JR-1 glasses synthesized from GSJ rock reference powder and a single crystal olivine from San Carlos, U.S.A. The JB-1a glass was used for calculation of secondary ion yield for all elements. The JR-1 glass and San Carlos olivine were used for interference corrections for P and Sc, and for Ni, respectively. Detected secondary ion intensities were corrected for natural isotopic abundances and normalized to the intensity of Si (reference mass ^{30}Si). Calibrations and corrections of concentrations from the secondary ion intensities have been described elsewhere (Yurimoto et al. 1989, 1991). Their sensitivity factors for elements were determined by the standard materials for every measurement. Typical values are shown in Table 2 with measurement masses and elemental abundances of the standards.

Results

Equilibrium consideration

Evaluation of chemical equilibrium is one of the most important factors in measuring partition coefficients.

[1] At present this instrument is installed in Laboratory for Planetary Sciences, Tokyo Institute of Technology.

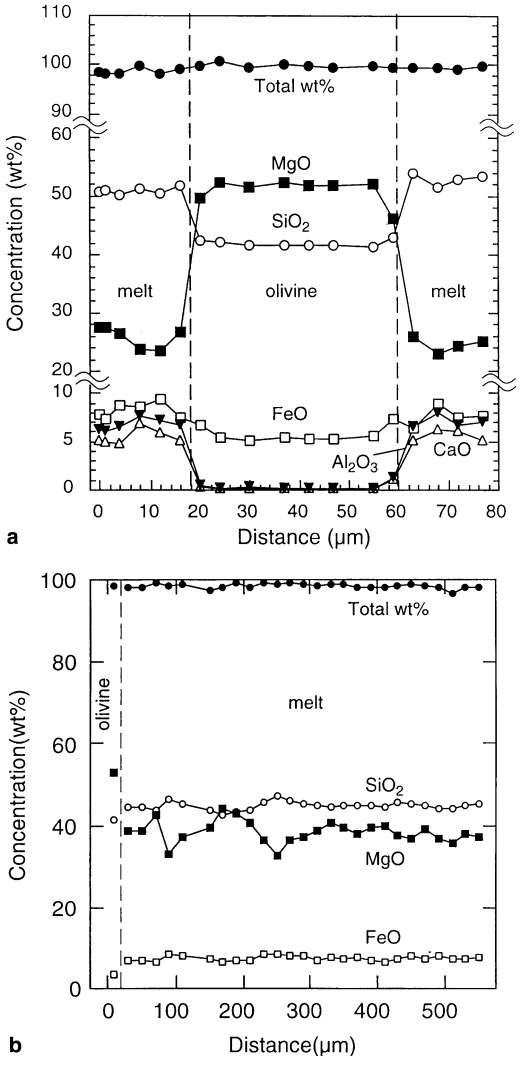

Fig. 1 **a** The compositional profile across olivine-melt boundary of KLB-17 by EPMA. *Dotted lines* denote olivine-melt boundaries. The beam size was set to about 3 μm in diameter. Concentrations of each element are homogeneous inside the olivine phenocryst, but some compositional gradients are observed both sides adjacent to the olivine-melt boundaries. **b** The compositional profile of KLB-43 by EPMA. The beam size was set to about 20 μm in diameter. The compositional fluctuations are due to the roughness of sample surface

Degree of partial melt and the run duration may control the attainment of chemical equilibrium in each run charge. All runs except for the KLB-25 showed the presence of a large amount of liquid phase (>50%) from mass balance calculation (olivine-liquid), i.e., the high-temperature condition easily approached equilibrium between olivine and liquid. The long run duration (25–60 min) for runs below 7 GPa was also important to reach chemical equilibration. Although the higher-pressure runs were made with a relative short run duration (5–10 min), e.g., the run duration of KLB-43 was 5 minutes, compositional distribution within olivine and quenched liquid may show that chemical equilibrium was achieved under high $P-T$ conditions.

Table 3 Average concentrations (wt%) of each phase in run charges determined by EPMA analysis[a]

Run	KLB-22		KLB-28		KLB-23		KLB-17		KLB-15		KLB-20	
Phase n=	olivine 28	Liquid 13	olivine 12	Liquid 19	olivine 5	Liquid 9	olivine 18	Liquid 11	olivine 16	Liquid 10	olivine 8	Liquid 8
SiO_2	41.24±0.21	48.74±0.66	41.22±0.24	46.33±0.83	41.68±0.17	47.70±0.47	41.43±0.15	47.06±0.53	41.49±0.12	47.36±0.40	42.04±0.17	46.76±0.58
Al_2O_3	0.15±0.01	7.09±0.29	0.13±0.01	5.01±0.58	0.22±0.04	6.09±0.24	0.19±0.01	5.76±0.27	0.20±0.02	5.51±0.27	0.19±0.02	5.27±0.71
TiO_2	0.01±0.01	0.23±0.02	0.01±0.01	0.15±0.02	0.01±0.004	0.20±0.02	0.01±0.005	0.19±0.02	0.01±0.01	0.17±0.02	0.01±0.01	0.17±0.02
Cr_2O_3	0.18±0.02	0.42±0.03	0.11±0.02	0.38±0.03	0.21±0.04	0.47±0.04	0.18±0.02	0.48±0.03	0.17±0.01	0.42±0.02	0.17±0.03	0.45±0.03
FeO	5.56±0.09	8.39±0.19	3.63±0.09	7.96±0.31	5.43±0.21	8.70±0.19	5.25±0.08	8.25±0.33	5.03±0.08	8.46±0.15	4.35±0.04	7.96±0.33
NiO	0.11±0.01	0.05±0.01	0.11±0.02	0.09±0.01	0.11±0.02	0.07±0.02	0.06±0.01	0.03±0.01	0.12±0.02	0.07±0.02	0.10±0.03	0.06±0.02
MnO	0.07±0.01	0.15±0.03	0.07±0.01	0.16±0.01	0.08±0.03	0.17±0.03	0.09±0.01	0.16±0.02	0.07±0.02	0.17±0.02	0.06±0.01	0.14±0.03
MgO	51.60±0.17	26.16±1.20	52.80±0.29	34.65±2.21	51.73±0.18	29.56±0.70	51.65±0.21	29.68±0.98	51.95±0.22	32.04±1.01	53.29±0.18	33.73±2.33
CaO	0.20±0.01	6.34±0.33	0.17±0.01	3.96±0.49	0.18±0.02	5.10±0.20	0.18±0.01	4.68±0.22	0.20±0.02	4.25±0.25	0.17±0.02	4.13±0.53
Na_2O	0.02±0.01	0.57±0.03	0.02±0.01	0.35±0.05	0.03±0.01	0.51±0.04	0.04±0.01	0.44±0.03	0.03±0.01	0.41±0.03	0.02±0.01	0.39±0.08
K_2O	0.01±0.003	0.05±0.01	0.02±0.01	0.03±0.01	0.02±0.01	0.06±0.01	0.01±0.004	0.05±0.01	0.01±0.003	0.03±0.01	0.004±0.01	0.04±0.01
Total	99.16	98.21	98.29	99.08	99.69	98.62	99.10	96.78	99.29	98.90	100.40	99.09
Oxygen=	4	59.58	4	58.78	4	59.23	4	59.24	4	59.05	4	58.88
Si	1.000	17.56	0.999	16.39	1.004	17.07	1.003	17.12	1.002	16.85	1.001	16.55
Al	0.004	3.01	0.004	2.09	0.006	2.57	0.005	2.47	0.006	2.31	0.005	2.20
Ti	0.001	0.24	0.002	0.19	0.001	0.22	0.001	0.22	0.001	0.19	0.001	0.20
Cr	0.004	0.12	0.002	0.11	0.004	0.13	0.003	0.14	0.003	0.12	0.003	0.13
Fe	0.113	2.53	0.074	2.36	0.109	2.60	0.106	2.51	0.101	2.52	0.087	2.35
Ni	0.002	0.01	0.002	0.02	0.002	0.02	0.001	0.01	0.002	0.02	0.002	0.02
Mn	0.002	0.05	0.001	0.05	0.002	0.05	0.002	0.05	0.002	0.05	0.001	0.04
Mg	1.864	14.04	1.907	18.26	1.856	15.76	1.863	16.09	1.868	16.97	1.890	17.78
Ca	0.005	2.45	0.004	1.50	0.005	1.95	0.005	1.82	0.005	1.62	0.004	1.57
Na	0.001	0.40	0.001	0.24	0.001	0.35	0.002	0.31	0.001	0.29	0.001	0.27
K	0.000	0.02	0.000	0.02	0.001	0.03	0.000	0.02	0.000	0.01	0.000	0.02
Total	2.995	100	2.997	100	2.991	100	2.993	100	2.993	100	2.995	100
$K_D^{Fe/Mg}$	0.34		0.30		0.36		0.37		0.37		0.35	

Table 3 (continued)

Run	KLB-25		KLB-13		KLB-35		KLB-31		KLB-43	
Phase n=	olivine 13	Liquid 7	olivine 31	Liquid 15	olivine 7	Liquid 7	olivine 4	Liquid 5	olivine 13	Liquid 23
SiO_2	41.60±0.25	48.01±1.12	41.97±0.12	46.40±0.25	41.51±0.28	46.59±0.42	41.90±0.24	45.32±0.32	41.76±0.20	44.64±0.41
Al_2O_3	0.23±0.02	5.63±0.58	0.19±0.01	5.46±0.23	0.26±0.02	5.23±0.19	0.26±0.04	4.70±0.20	0.24±0.02	3.85±0.22
TiO_2	0.01±0.01	0.28±0.05	0.01±0.01	0.16±0.01	0.002±0.004	0.18±0.01	0.01±0.01	0.12±0.03	0.004±0.003	0.12±0.02
Cr_2O_3	0.16±0.02	0.48±0.03	0.13±0.02	0.47±0.02	0.16±0.03	0.46±0.05	0.13±0.03	0.44±0.05	0.07±0.02	0.34±0.03
FeO	6.11±0.17	9.55±0.64	4.50±0.11	8.29±0.16	4.94±0.13	8.78±0.25	3.73±0.17	7.90±0.35	3.23±0.06	7.62±0.28
NiO	0.15±0.02	0.07±0.03	0.06±0.01	0.05±0.01	0.17±0.02	0.12±0.03	0.24±0.01	0.17±0.01	0.11±0.01	0.14±0.01
MnO	0.09±0.01	0.20±0.03	0.07±0.01	0.16±0.02	0.07±0.02	0.16±0.03	0.03±0.01	0.14±0.03	0.05±0.01	0.13±0.01
MgO	50.21±0.24	24.19±2.60	52.39±0.17	31.53±0.60	52.22±0.17	32.56±0.47	53.06±0.38	36.83±0.73	53.62±0.24	37.54±0.84
CaO	0.22±0.02	7.57±0.87	0.14±0.01	4.60±0.17	0.15±0.02	4.03±0.23	0.16±0.01	3.39±0.13	0.13±0.01	3.11±0.23
Na_2O	0.04±0.01	0.62±0.12	0.02±0.01	0.39±0.03	0.05±0.02	0.40±0.03	0.04±0.01	0.35±0.00	0.05±0.01	0.31±0.03
K_2O	0.01±0.005	0.02±0.02	0.01±0.003	0.04±0.01	0.004±0.004	0.01±0.01	0.01±0.01	0.02±0.01	0.01±0.01	0.01±0.00
Total	98.84	96.62	99.50	97.54	99.52	98.53	99.56	99.38	99.26	97.81
Oxygen=	4	59.56	4	59.01	4	58.94	4	58.52	4	58.43
Si	1.013	17.75	1.008	16.75	1.000	16.65	1.003	15.97	1.001	15.95
Al	0.006	2.45	0.005	2.32	0.007	2.20	0.007	1.95	0.007	1.62
Ti	0.002	0.30	0.001	0.19	0.000	0.21	0.001	0.16	0.000	0.16
Cr	0.003	0.14	0.003	0.14	0.003	0.13	0.002	0.12	0.001	0.10
Fe	0.124	2.95	0.090	2.50	0.099	2.62	0.075	2.33	0.065	2.28
Ni	0.003	0.02	0.001	0.01	0.003	0.04	0.005	0.05	0.002	0.04
Mn	0.002	0.06	0.001	0.05	0.001	0.05	0.001	0.04	0.001	0.04
Mg	1.821	13.32	1.873	16.95	1.874	17.33	1.892	19.33	1.914	19.98
Ca	0.006	3.00	0.004	1.78	0.004	1.54	0.004	1.28	0.003	1.19
Na	0.002	0.44	0.001	0.27	0.002	0.28	0.002	0.24	0.002	0.22
K	0.000	0.01	0.000	0.02	0.000	0.00	0.000	0.01	0.000	0.01
Total	2.982	100	2.988	100	2.995	100	2.992	100	2.996	100
$K_D^{Fe/Mg}$	0.31		0.33		0.35		0.33		0.30	

[a] n: number of EPMA analysis from different positions in each phase. The lower half of this table shows calculated cation numbers for olivine and atomic% for liquid. Error is presented as $\pm 2\,\sigma/\sqrt{n}$. $K_D^{Fe/Mg}$ is represented as $(C^{ol}/C^{liq})_{Fe}/(C^{ol}/C^{liq})_{Mg}$

Table 4 Concentrations (ppm) of each phase in run charges determined by SIMS analysis[a]

Run	KLB-22				KLB-28				KLB-23				KLB-17				KLB-15				KLB-20			
Phase	olivine	R.E.%	Liquid	R.E.%	olivine	R.E.%	Liquid	R.E.%	olivine	R.E.%	Liquid	R.E.%	olivine	R.E.%	Liquid	R.E.%	olivine	R.E.%	Liquid	R.E.%	olivine	R.E.%	Liquid	R.E.%
Li	4.6		13.9		0.7	10%	3.5		4.8		10		2.8		5.8		1.3		3.3		1.2	8%	2.2	
Be	n.d.		n.d.		n.d.		n.d.		n.d.		0.5		n.d.		n.d.		n.d.		0.4		n.d.		0.3	
B	4.5	9%	602		2.4	14%	73		14		726		0.9	11%	19		2.0	13%	50		4.8	12%	134	
Na	143		3892		97		2466		196		4097		174		3238		202		3130		239		3030	
Mg	236300		139200		250000		180900		227100		138800		239805		153200		225900		154500		233400		154700	
Al	738		37770		639		22830		958		35640		952		31690		1101		27880		964		27180	
Si	192800		227900		192700		216600		194800		223000		193700		220000		194000		221400		196500		218600	
P	9.8	14%	54		70		64		62		64		140		133		122		220		162		288	
K	29	6%	501		132		231		4.7	9%	559		1.7	11%	369		6.9	9%	296		20	12%	438	
Ca	1100		40300		1005		25640		1032		38310		1002		32930		1135		28870		1026		27960	
Sc	4.0		18		2.8		17		2.9		24		3.6		27		3.6		21		3.7		21	
Ti	22	12%	1512		18	12%	776		16.8	7%	1359		19		1236		27	7%	1021		16	13%	1033	
V	30		120		19		87		23		130		21		111		25		106		18		105	
Cr	1042		2246		1111		3001		1183		3543		1045		2927		1081		2966		964		2905	
Mn	569		1210		382		985		497		1251		484		1190		448		1095		415		1035	
Fe	42120		65600		24550		55180		35930		67620		33818		66600		32080		62060		28420		57710	
Co	63		54		42		53		52		56		51		58		53		62		48		49	
Ni	1320		452		850		755		911		456		505		268		854		672		941		536	
Cu	5.1	18%	61		10.9	15%	64		7.8	11%	96		3.9	10%	43		6.6	12%	67		7.5	17%	58	
Rb	n.d.		7.0	6%	n.d.		5.3	7%	n.d.		6.7	8%	n.d.		5.9	6%	n.d.		6.1	8%	n.d.		5.6	8%
Sr	0.2	52%	34		n.d.		8.6		0.1	58%	11		0.1	50%	12		0.2	38%	11		n.d.		8.9	
Y	0.2	39%	7.4		0.2	45%	4.0		0.1	45%	7.1		n.d.		6.4		n.d.		5.3		0.2	41%	4.6	
Zr	0.5	39%	259		0.5	41%	206		0.7	20%	899		0.2	41%	370		0.9	25%	362		0.6	41%	44	
Cs	n.d.		0.8	27%	n.d.		1.2	16%	n.d.		n.d.		n.d.		1.3	14%	n.d.		1.9	20%	n.d.		1.5	23%
Ba	1.6	27%	174		n.d.		4.7	6%	n.d.		8.5		0.1	50%	6.4		n.d.		5.3	6%	n.d.		4.7	8%
La	0.4	38%	15		0.4	41%	31		0.1	50%	619		n.d.		1.4	7%	n.d.		3.1	7%	n.d.		99	
Ce	0.1	58%	4.0		n.d.		0.7	12%	n.d.		3.0	6%	n.d.		1.0	10%	n.d.		1.1	11%	n.d.		1.5	10%

[a] An olivine crystal and liquid area were selected for each run product from results of equilibrium consideration by EPMA analyses. R.E.%: Standard deviation calculated from counting statics, which is larger than 5%. n.d.: not detected.

Table 4 (continued)

Run	KLB-25				KLB-13				KLB-35				KLB-31				KLB-43			
Phase	olivine	R.E.%	Liquid	R.E.%	olivine	R.E.%	Liquid	R.E.%	olivine	R.E.%	Liquid	R.E.%	olivine	R.E.%	Liquid	R.E.%	olivine	R.E.%	Liquid	R.E.%
Li	6.7		14		4.1		9.8		1.1		1.9		1.0		1.8		0.9	9%	1.9	
Be	n.d.		0.3	6%	n.d.		0.03	18%	n.d.		0.02	10%	0.02	27%	0.3		n.d.		0.02	21%
B	63		2584		12		689		0.4	12%	18		2.2	10%	18		1.8	15%	14	
Na	346		4167		198		2681		310		2814		357		2787		343		2002	
Mg	217700		161800		247000		161000		239800		166300		225200		169200		243100		177700	
Al	1056		27780		999		30150		1154		27350		1388		24570		1092		21130	
Si	194500		224400		196200		216900		194000		217800		195900		211800		195200		208700	
P	256		227		9.5	6%	41		79		73		51		157		193		279	
K	9.8	9%	268		1.2	15%	365		0.3	19%	94		7.0	7%	68		2.8	14%	2	
Ca	1214		44410		915		31610		941		27990		1026		24100		783		23340	
Sc	3.8		28		2.1		24		2.2		24		2.4		19		3.0		20	
Ti	17	14%	1914		10	9%	1311		14		1304		8.1	17%	1047		10	16%	780	
V	20		145		16		107		17		102		15		95		13		88	
Cr	909		3001		838		2922		831		2809		774		2859		723		3109	
Mn	529		1494		398		1091		432		1164		385		1050		332		1011	
Fe	39520		98000		27480		61160		30420		67660		26470		61170		22620		59570	
Co	61		92		38		51		63		75		52		70		42		71	
Ni	1253		978		483		353		1571		1074		1827		1256		988		1196	
Cu	15	12%	94		10	7%	143		2.3	11%	41		1.2	27%	20		2.1	31%	17	
Rb	n.d.		9.8	8%	n.d.		6.5	6%	n.d.		4.3		n.d.		5.8	8%	n.d.		4.5	7%
Sr	0.3	45%	12		0.03	71%	19		0.2	17%	8.9		0.3	24%	7.0		0.3	40%	6.6	
Y	0.1	58%	7.0		0.1	41%	5.6		0.02	45%	5.8		n.d.		4.4		0.1	100%	3.8	
Zr	0.5	50%	1105		0.7	19%	2125		0.1	38%	107		n.d.		135		0.1	100%	14	
Cs	n.d.		n.d.		n.d.		n.d.		n.d.		0.3	23%	n.d.		n.d.		n.d.		0.8	21%
Ba	n.d.		12	6%	0.1	71%	95		0.04	58%	2.1		n.d.		4.4	8%	n.d.		2.2	9%
La	n.d.		114		n.d.		16		n.d.		13		0.1	50%	1182		n.d.		1.4	7%
Ce	n.d.		3.2	9%	n.d.		3.9		n.d.		n.d.		n.d.		4.4	6%	n.d.		0.7	12%

Typical compositional profiles of major elements across the boundary between olivine and melt are shown in Fig. 1a, b. A homogeneous distribution was observed within both the olivine and quenched melt phases. However, a depletion of MgO content is observed in the melt region adjacent to the olivine/melt boundary, and normal zoning is observed in the rim of olivine phenocrysts (Fig. 1a). This zoning indicates that the rim of olivine was overgrown during the quenching process, so that the adjacent melt was depleted in olivine components. The disequilibrium zones were restricted to a region less than 10 μm from the boundary. Thus, measurements in the center of crystals give accurate results for determining equilibrium partition coefficients.

The compositional profiles in the liquid phase across the capsule are shown in Fig. 1b. The compositional fluctuation displayed in the figure is due to the hole of the sample surface. The measurements for quenched liquid were avoided on such rough-surface regions. The homogeneous composition of quenched liquid in the capsule indicated that the quenching of the run charge preserved chemical composition at high-pressure and high-temperature conditions. These line profiles showed clearly that the disequilibrium region was only the rim of olivine crystals and the quenched liquid around them.

In addition, the exchange partition coefficients, $K_{D_{Fe/Mg}}^{ol/liq}$, support the chemical equilibrium of each run product. $K_{D_{Fe/Mg}}^{ol/liq}$ are in the range from 0.30 to 0.37 (Table 3). These values are consistent with other high-pressure experiments (e.g. 0.33±0.06 by Zhang and Herzberg 1996).

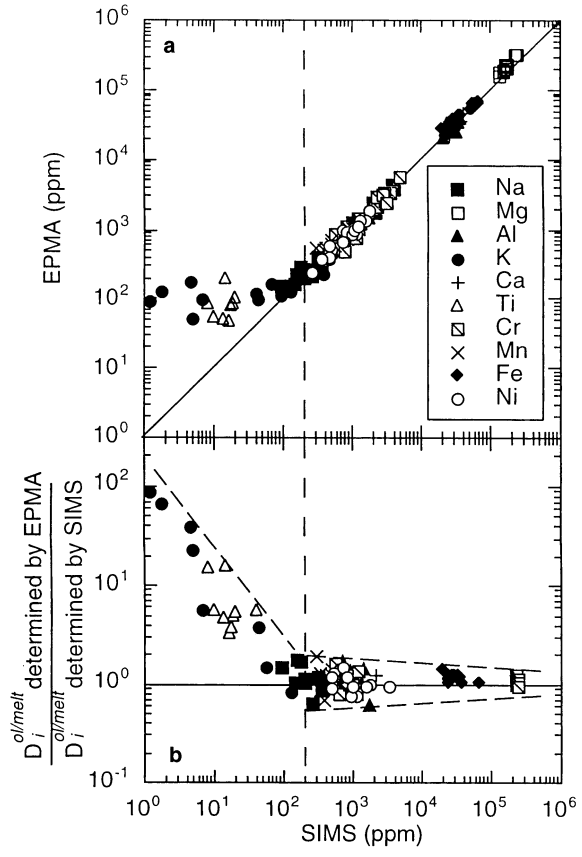

Fig. 2a, b Comparison between analytical results of EPMA and SIMS. **a** Correlation between concentrations of olivine and melt phases determined by SIMS and EPMA. **b** Ratio of olivine/melt partition coefficient determined by EPMA and SIMS vs concentration of olivine phase determined by SIMS

Analytical results

The concentrations of 11 major elements determined by EPMA are listed in Table 3, and the abundances of 27 elements determined by SIMS are listed in Table 4.

The uncertainties of EPMA analysis are represented by $2\sigma/\sqrt{n}$. The uncertainties of MgO in olivine are below 0.4 wt%. It implies the homogeneity of olivine crystals of each run. The uncertainties of MgO in liquid are below 3 wt% (typically below 1 wt%), which are slightly larger than those of olivine. These are because the liquid phase is composed of the dendritic quenched crystals. The average compositions of quenched liquids were well determined (less than 5% accuracy) in these analytical conditions.

Concentrations of elements determined by both EPMA and SIMS are compared in Fig. 2. For major elements, there is a linear correlation with a slope of unity between the two methods, whereas, elements present at the sub-ppm level deviate significantly upwards from the slope of unity. Such deviation is due to the effect of background noise in EPMA analysis causing a significantly higher detectibility limit.

The partition coefficient, $D_i^{ol/melt}$, is defined as the ratio of elemental concentration, C_i^{ol}/C_i^{melt}, where C_i^{ol} and C_i^{melt} represent the concentration of element i in olivine and melt, respectively. Partition coefficients determined by EPMA and SIMS are compared in Fig. 2b. Differences between partition coefficients determined by the two methods are not apparent for major elements; however, systematic differences are clearly apparent for trace elements. The systematic differences are ascribed to the detection limitis of EPMA.

We should note that $D_{Mg}^{ol/melt}$ and $D_{Fe}^{ol/melt}$ determined by EPMA are slightly larger than those determined by SIMS (Fig. 2). The small discrepancy may come from improper corrections for the matrix effects of SIMS, i.e., secondary ion yield of olivine crystal is lower than that of quench crystals. Difference of secondary ion yield between olivine and melt phases of run products may be evaluated by comparing those between San Carlos olivine and the JB-1a glass standards because the chemical compositions of each phase in the run products are distributed within the compositional range of the standard materials. The olivine/glass ratios of secondary ion yield between the standards are 0.73 for Mg, 0.78 for Fe and 0.84 for Mn. The ion yield is enhanced by the oxygen abundance on its matrix generally (e.g. Benninghoven et al. 1986). Olivine contained oxygen (57 atomic%), which is lower than

Table 5 Partition coefficients between olivine and melt determined by SIMS analysis[a]

Element	KLB-22		KLB-28		KLB-23		KLB-17		KLB-15		KLB-20		KLB-25		KLB-13		KLB-35		KLB-31		KLB-43	
	$D^{ol/melt}$	R.E.%	$D^{ol/melt}$	R.E.%	$D^{ol/melt}$	R.E.%	$D^{ol/melt}$	R.E.%	$D^{ol/melt}$	R.E.%	$D^{ol/melt}$	R.E.%	$D^{ol/melt}$	R.E.%	$D^{ol/melt}$	R.E.%	$D^{ol/melt}$	R.E.%	$D^{ol/melt}$	R.E.%	$D^{ol/melt}$	R.E.%
Li	0.33		0.21	10%	0.47		0.48		0.40		0.54	8%	0.49		0.417		0.56		0.55		0.45	10%
B	0.007	10%	0.032	14%	0.019		0.047	11%	0.040	13%	0.036	12%	0.024		0.018		0.022	12%	0.119	10%	0.125	21%
Na	0.037		0.040		0.048		0.054		0.065		0.079		0.083		0.074		0.11		0.13		0.17	
Mg	1.70		1.38		1.64		1.57		1.46		1.51		1.35		1.53		1.44		1.33		1.37	
Al	0.020		0.028		0.027		0.030		0.039		0.035		0.038		0.033		0.042		0.056		0.052	
Si	0.85		0.890		0.87		0.88		0.88		0.90		0.87		0.90		0.89		0.92		0.94	
P	0.18	10%	1.08	6%	0.98		1.05		0.55		0.56		1.17		0.23	6%	1.09		0.33		0.69	
K	0.058		0.57		0.008	9%	0.005	11%	0.023	9%	0.047	12%	0.037	9%	0.003	15%	0.004	19%	0.103	7%	0.067	15%
Ca	0.027		0.039		0.027		0.030		0.039		0.037		0.027		0.029		0.034		0.043		0.034	
Sc	0.22		0.17		0.12		0.13		0.17		0.17		0.14		0.088		0.093		0.12		0.15	
Ti	0.014	13%	0.023	12%	0.012	7%	0.015		0.026	7%	0.016	13%	0.009	14%	0.008	9%	0.010		0.008	17%	0.013	17%
V	0.25		0.22		0.18		0.19		0.23		0.17		0.14		0.15		0.17		0.16		0.15	
Cr	0.46		0.37		0.33		0.36		0.36		0.33		0.30		0.29		0.30		0.27		0.23	
Mn	0.47		0.39		0.40		0.41		0.41		0.40		0.35		0.36		0.37		0.37		0.33	
Fe	0.64		0.44		0.53		0.51		0.52		0.49		0.40		0.45		0.45		0.43		0.38	
Co	1.17		0.79		0.93		0.87		0.85		0.99		0.67		0.75		0.83		0.74		0.59	
Ni	2.92	6%	1.13		2.00		1.88		1.27		1.76		1.28		1.37		1.46		1.45		0.83	
Cu	0.083	17%	0.170	15%	0.081	11%	0.092	10%	0.098	12%	0.13	17%	0.16	12%	0.073	8%	0.056	11%	0.059	27%	0.12	36%
Sr	0.006	42%	0.091	27%	0.005	58%	0.005	50%	0.020	38%	0.061	29%	0.024	45%	0.002	71%	0.020	17%	0.0047	24%	0.052	35%
Y	0.025	43%	0.045	45%	0.008	45%	n.d.		n.d.		0.044	41%	0.016	58%	0.010	41%	0.003	45%	n.d.		0.013	10%
Zr	0.002	42%	0.002	41%	0.001	20%	0.0004	41%	0.003	25%	0.013	41%	0.0004	50%	0.0003	19%	0.001	38%	n.d.		n.d.	
Ba	0.009	33%	n.d.		n.d.		0.014	50%	n.d.		n.d.		n.d.		n.d.		0.018	58%	n.d.		n.d.	
La	0.029	45%	0.014	41%	0.0002	50%	n.d.		n.d.		n.d.		n.d.		n.d.		n.d.		n.d.		n.d.	
Ce	0.015		n.d.		n.d.		n.d.		n.d.		n.d.		n.d.		n.d.		n.d.		n.d.		n.d.	

[a] R.E.%: Standard deviation calculated from counting statistics, which is larger than 5%. n.d.: not detected

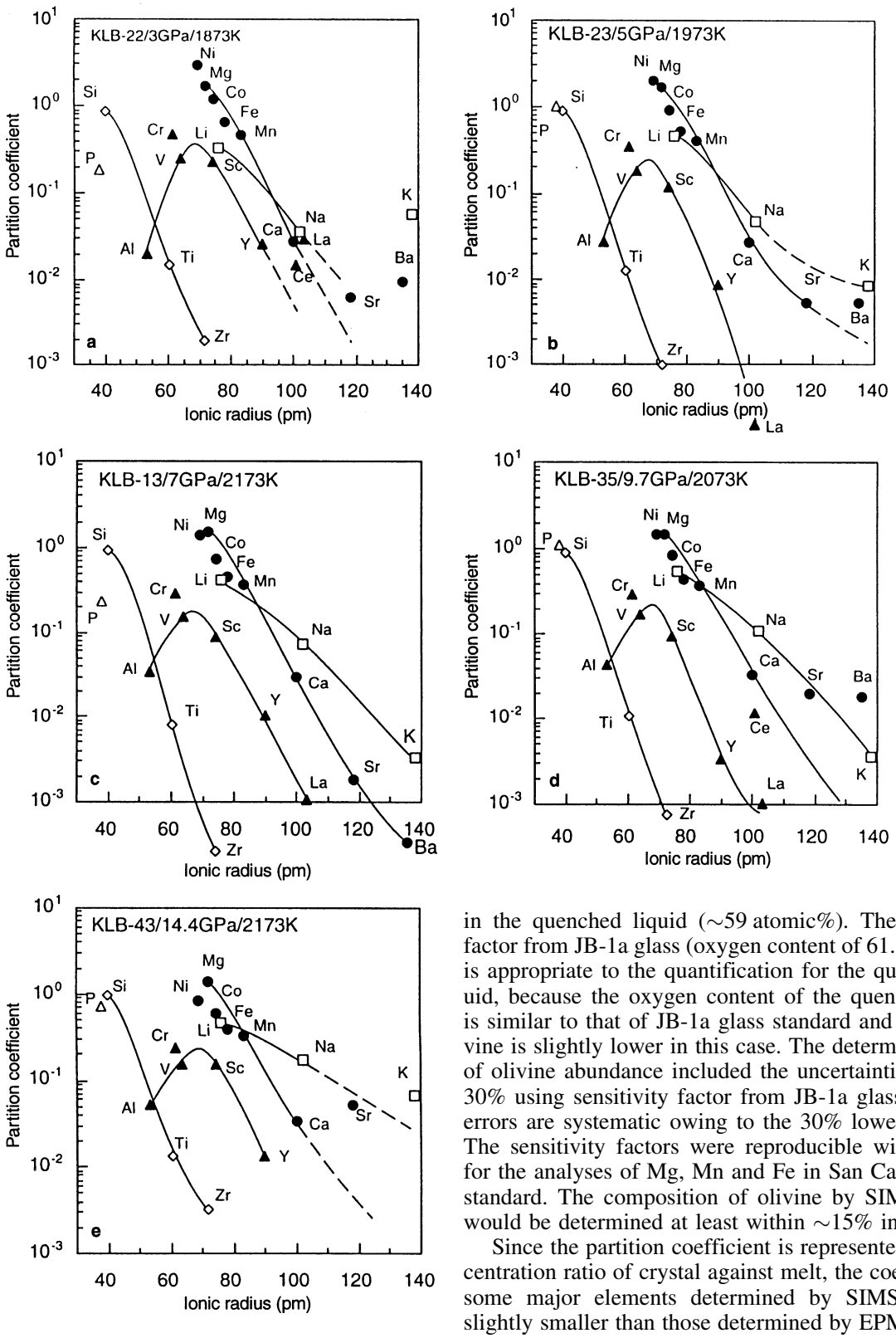

Fig. 3a–e Onuma diagrams of olivine/melt system at pressures from 3 to 14.4 GPa. Parabola shaped lines are connected among isovalent cations. *Open square* monovalent cations, *solid circle* divalent cations, *solid triangle* trivalent cations, *open diamond* tetravalent cations, *open triangle* pentavalent cations

in the quenched liquid (~59 atomic%). The sensitivity factor from JB-1a glass (oxygen content of 61.8 atomic%) is appropriate to the quantification for the quenched liquid, because the oxygen content of the quenched liquid is similar to that of JB-1a glass standard and that of olivine is slightly lower in this case. The determined values of olivine abundance included the uncertainties of about 30% using sensitivity factor from JB-1a glass, but these errors are systematic owing to the 30% lower ion yield. The sensitivity factors were reproducible within ~15% for the analyses of Mg, Mn and Fe in San Carlos olivine standard. The composition of olivine by SIMS analysis would be determined at least within ~15% in precision.

Since the partition coefficient is represented by a concentration ratio of crystal against melt, the coefficient for some major elements determined by SIMS might be slightly smaller than those determined by EPMA because of lower secondary ion yield of olivine crystals as compared with quenched crystals. If $D_i^{ol/melt}$ by SIMS analysis trends to give a slightly smaller value than that by EPMA analysis, the discrepancies between them are estimated to be less than 30% on the basis of the standard analysis. The discrepancies are permissible on the log scale diagram

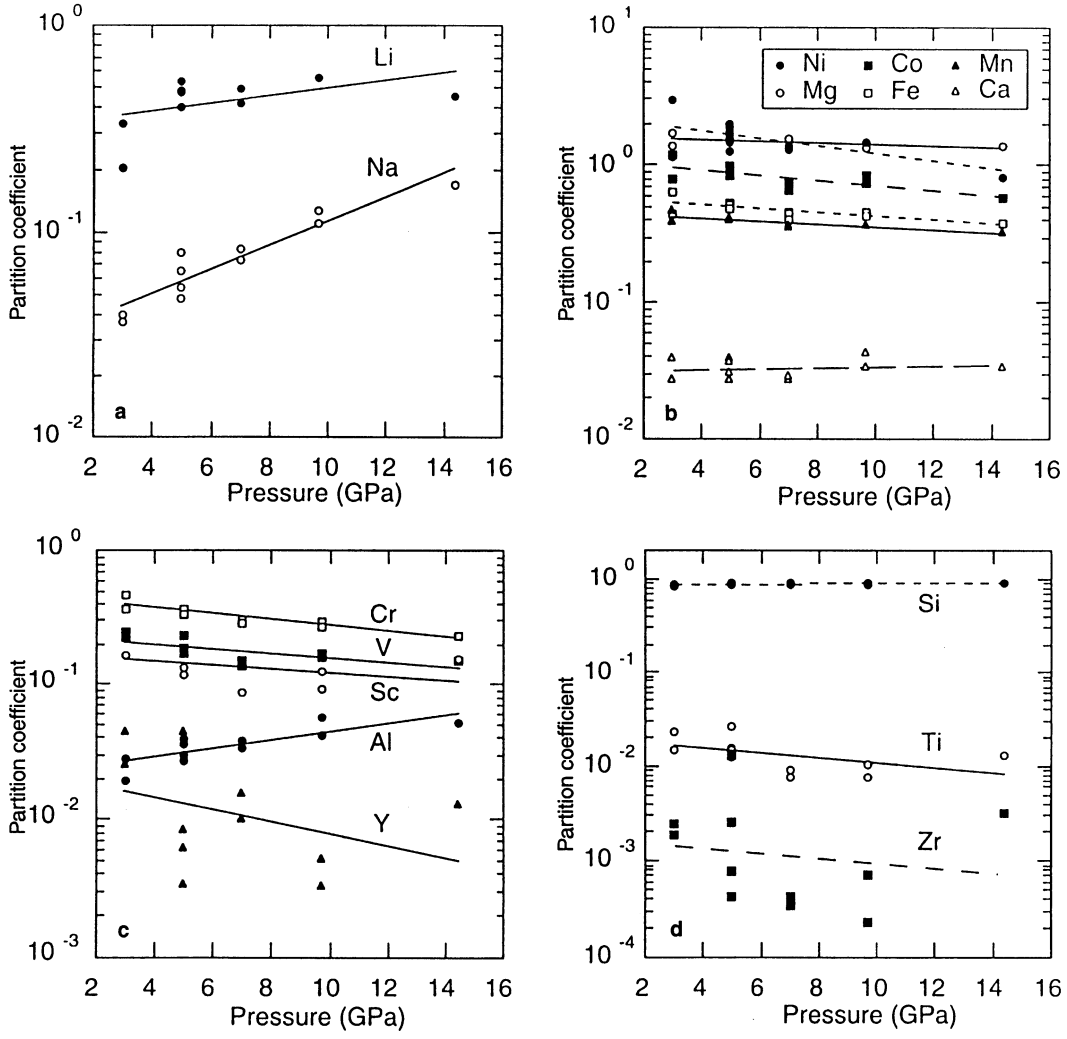

Fig. 4a–d Plots of olivine/melt partition coefficients vs pressure. **a** monovalent cations, **b** divalent cations, **c** trivalent cations, **d** tetravalent cations. Lines are exponential curves fitted by least squares method

such as the Onuma diagrams (Onuma et al. 1968) used below (Fig. 3). Thus, we use the concentrations determined by SIMS analysis to calculate partition coefficients for all elements. Partition coefficients are listed in Table 5.

Partition coefficients for K, Ba and Sr sometimes deviate upward from the smooth curves in Fig. 3. These elements easily contaminated the sample surface during polishing in spite of careful treatment of sample preparation. Since abundances of these elements in olivine are extremely small, then it is difficult to remove the surface contamination perfectly by pre-sputtering of SIMS analysis, especially in use of the micro-size primary-ion beam in this study. The small degree of the contamination introduced overestimation of the partition coefficient.

Onuma diagram of olivine/melt system

Partition coefficients between olivine and coexisting melt are plotted against ionic radius on Fig. 3, and using a six coordinated set by Shannon (1976). This diagram is called a "PC-IR" or "Onuma" diagram (Onuma et al. 1968). Fig. 3 shows Onuma diagrams for the olivine/melt system at pressures of 3 to 14.4 GPa. Curves connecting isovalent cations show similar patterns to those observed in the olivine-melt systems at low pressure (Matsui et al. 1977; Yurimoto and Sueno 1984), that is, the partition coefficients are essentially controlled by the crystal structure of olivine even at high pressure.

The stoichiometry of olivine is represented by M_2TO_4, which means that the olivine structure is composed of two cation sites, at four coordinated T site and a six coordinated M site (Birle et al. 1968). The M and T sites are occupied mainly by divalent and tetravalent cations, respectively. The tetravalent cations Si, Ti and Zr make a smooth curve for T-site occupation on Onuma diagrams (Fig. 3) and the partition coefficients for each cation are almost constant over the range of experimental pressures (Fig. 4). The curve drawn through the divalent cations Ni, Mg, Co, Fe, Mn and Ca indicates an M-site parabola, although Ni, Co and Fe deviate from the smooth curve for the M-site (Fig. 3). The reason for this deviation is due to crystal field effects of these cations (Matsui et al. 1977). Partition coefficients of Mg, Mn and Ca are almost con-

stant over the pressure range, but those of Ni, Co and Fe gradually decrease with pressure (Fig. 4).

The trivalent cations Al, V, Sc and Y form a complete parabola for M site occupations. $D_{Cr}^{ol/melt}$ deviates upward from the trivalent parabola due to crystal field effects. The partition coefficient of Al increases with pressure, while partition coefficients of other trivalent cations such as Cr, V, Sc and Y decrease with pressure (Fig. 4). Abundances of La and Ce in olivine are extremely small so that their abundances were not determined precisely by SIMS.

A monovalent curve is drawn for Li and Na. The curve forms the right half side of an M site parabola (Fig. 3). Partition coefficients of Li and Na increase with pressure (Fig. 4) and the rate of increase for Na is larger than that for Li.

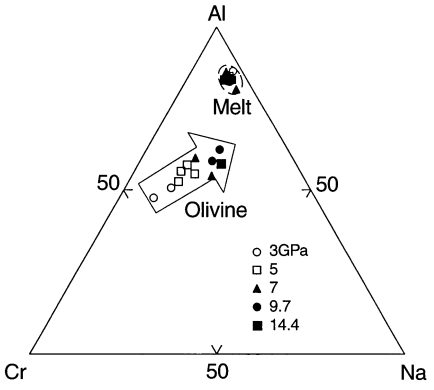

Fig. 5 Ternary plot of Al, Cr and Na in olivine and in the coexisting melts

Discussion

Substitution of mono- and tri-valent cations in olivine

The two cation sites (M and T) in the olivine structure are occupied mainly by di- and tetra-valent cations. Thus, only trace quantities of mono- and tri-valent cations substitute with the host cations. Major species of tri- and monovalent cations in olivine crystals of the run products are Al^{3+}, Cr^{3+} and Na^{+} owing to their relatively high abundances in the natural peridotite starting material, KLB-1. The abundances of other mono- and tri-valent cations in olivine crystals were less than several tens of ppm (Table 4). Therefore, the style of site substitution for mono- and tri-valent cations in olivine could be examined by the three cations Al, Cr and Na. Atomic proportions of Al, Cr and Na against (Al+Cr+Na) in olivine and in melt are plotted in a ternary diagram (Fig. 5). The proportion of both Al and Na in olivine increases with pressure, whereas Cr decreases. The proportions of these elements in coexisting melts plot in a small region. These results indicate that the partitioning of these trace elements is controlled by a substitution mechanism into the olivine structure. On the basis of Pauling's second rule, substitution of mono- and tri-valent cations in olivine must neutralize their formal charges in order to occupy the sites.

Ozawa (1991) proposed the following conditions for trace element substitution in olivine:

(1) Na^{+} occupies only the M site because of its larger ionic radius relative to the position of the M site parabola peak.
(2) Cr^{3+} also occupies only the M site because of its similar ionic radius to the M site parabola peak and the crystal field effect.
(3) Al^{3+} occupies both the M and T sites because it's ionic radius lies between parabola peaks of the M and T sites.
(4) Vacancies do not play an important role in cation substitutions at high pressure.

According to this formulation, four structural formulas were introduced for cationic substitution.

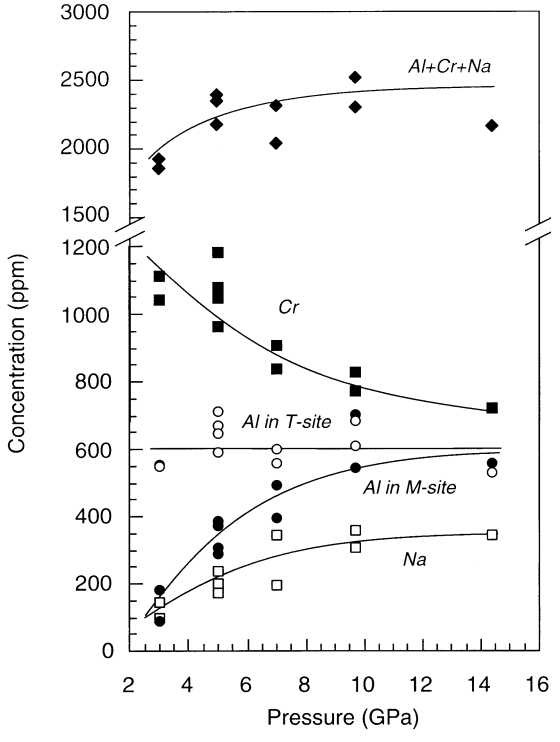

Fig. 6 Abundances of Al_T, Al_M, Cr and Na as a function of pressure

$$Mg^{2+}Cr^{3+}Al_T^{3+}O_4 \quad (1)$$

$$Mg^{2+}Al_M^{3+}Al_T^{3+}O_4 \quad (2)$$

$$Na^{+}Al_M^{3+}Si^{4+}O_4 \quad (3)$$

$$Na^{+}Cr^{3+}Si^{4+}O_4 \quad (4)$$

where the subscripts M and T denote the crystallographic sites of the olivine structure. Combining Eqs. 1, 2, 3 and 4, we find that the total number of substituting cations, [Al]+[Cr]+[Na], can be expressed as

$$[Al]+[Cr]+[Na]=2([Al^{3+}]_T+[Na^{+}]) \quad (5)$$

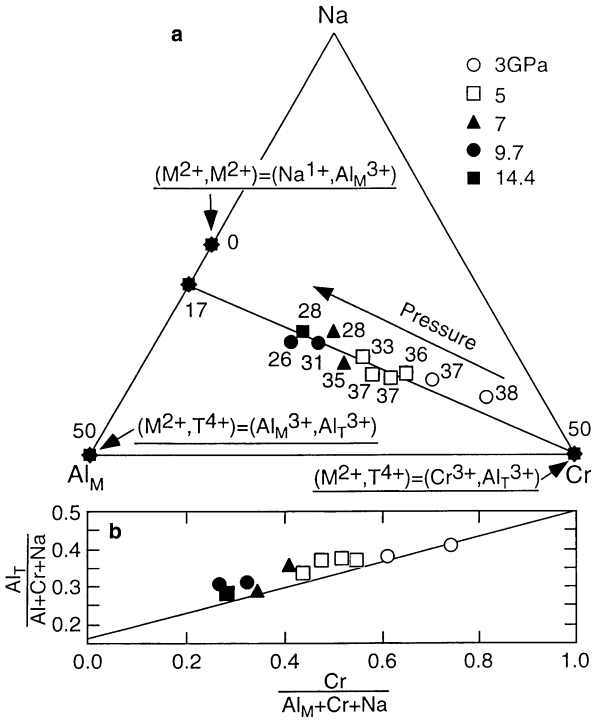

Fig. 7a, b Site occupancy among Al^{3+}, Cr^{3+}, and Na^{+}. **a** Projection onto the Al_M–Cr–Na plane from Al_T in the Al_T–Al_M–Cr–Na tetrahedron. Numbers in the projection plot are ratios (%) of Al_T/(Na+Al+Cr). Solid line connects (Al_T, Al_M, Cr, Na)=(0.5, 0, 0.5, 0) with (Al_T, Al_M, Cr, Na)=(0.17, 0.5, 0, 0.33). **b** Plot of Cr/(Al_M+Cr+Na) vs Al_T/(Al+Cr+Na)

where [Al] is the atomic fraction of Al, for example. Therefore, $[Al^{3+}]_T$ and $[Al^{3+}]_M$ are derived from the atomic fraction of Al, Cr and Na:

$$[Al^{3+}]_T=([Al]+[Cr]-[Na])/2 \quad (6)$$

$$[Al^{3+}]_M=([Al]-[Cr]+[Na])/2. \quad (7)$$

Using these equations, the concentration of Al, Cr and Na in olivine can be deconvoluted to those for each crystallographic site.

Figure 6 shows that the amount of Al^{3+} in the T-site remains nearly constant over the pressure range. The Al^{3+} contents in M-sites increases significantly with pressure, whereas the Cr^{3+} contents in M-sites decreases. The Na^{+} contents in M-sites also increase with pressure. Pressure dependence of site occupancies among Al^{3+}, Cr^{3+}, and Na^{+} in olivine is shown in Fig. 7. The points Cr=1, Al_M=1 and Al_M=Na=0.5 of Fig. 7a correspond to the substitution types (Si^{4+}, Mg^{2+})↔(Al^{3+}, Cr^{3+}), (Si^{4+}, Mg^{2+})↔(Al^{3+}, Al^{3+}) and (Mg^{2+}, Mg^{2+})↔(Na^{+}, Al^{3+}), respectively. The 3 GPa points are positioned at the Cr-rich side, and that at 14.4 GPa is positioned in the Cr-poor side. The ratio of [Cr]/($[Al]_M$+[Cr]+[Na]) decreases with pressure and those of $[Al]_M$/($[Al]_M$+[Cr]+[Na]) and [Na]/($[Al]_M$+[Cr]+[Na]) increase. These results indicate that (Si^{4+}, Mg^{2+})↔(Al^{3+}, Cr^{3+}) type substitutions are dominant in olivine at low pressure, but that the substitution type changes to (Si^{4+}, Mg^{2+})↔(Al^{3+}, Al^{3+}) and (Mg^{2+}, Mg^{2+})↔(Na^{+}, Al^{3+}) with increase in pressure. The substitution mechanism changes on the line linking the points (Al_T, Al_M, Cr, Na)=(0.5, 0, 0.5, 0) and (0.17, 0.5, 0, 0.33).

Figure 8 shows possible substitutions for the above four structural formulas. Substitution of Mg^{2+} Cr^{3+} $Al_T^{3+}O_4$ is dominant at low pressure. When Al^{3+} occupies the T-site in olivine, Cr^{3+} may substitute to the adjacent M2-site with a shared corner (Fig. 8a). Since the ionic radius of Al^{3+} is larger than that of Si^{4+}, and the ionic radius of Cr^{3+} is smaller than that of Mg^{2+}, M2 octahedra with Cr^{3+} become compacted, and T tetrahedron with Al^{3+} expand toward the M2-site of Cr^{3+}. These local modifica-

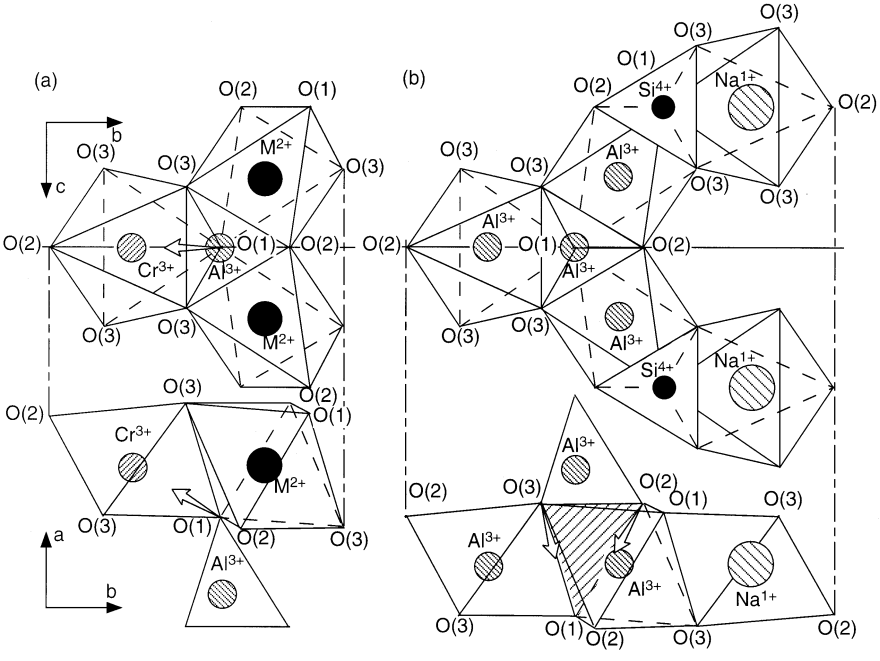

Fig. 8a, b Possible substitution types for tri- and mono-valent cations in olivine structure. **a** (Si^{4+}, Mg^{2+})↔(Al^{3+}, Cr^{3+}) type substitution, **b** (Si^{4+}, Mg^{2+})↔(Al^{3+}, Al^{3+}) and 2(Mg^{2+}, Mg^{2+})↔2(Na^{+}, Al^{3+}) type substitution

tions in the crystal structure stabilize the (Si^{4+}, Mg^{2+})↔(Al^{3+}, Cr^{3+}) type substitution at lower pressure.

At high pressure the (Si^{4+}, Mg^{2+})↔(Al^{3+}, Al^{3+}) and (Mg^{2+}, Mg^{2+})↔(Na^{+}, Al^{3+}) type substitutions become dominant. Although a decrease in cell volume is favored at high pressure, Al^{3+} substitutes to the tetrahedral site in olivine instead of Si^{4+} even at high pressures (Fig. 6). For formal charge neutralization, substitution of $Mg^{2+}Al^{3+}_{M}Al^{3+}_{T}O_4$ may reduce cell volume of the host olivine because of the small ionic radius of six-coordinated Al^{3+}. Figure 7 shows that the above two substitutions occur in the ratio of 1:2. This ratio indicates that substitution of one Al^{3+} in T-site carries with it the substitution of three Al^{3+} and two Na^{+} in M-site. Since Al^{3+} abundance in the T-site is not dependent on pressure and Cr^{3+} in the M2-site becomes unstable with pressure (Fig. 6), Al^{3+} and Na^{+} substitute to the M1- and M2-sites in place of Cr^{3+}. Accordingly four Al^{3+} substitute to one M2-site, two M1-sites and one T-site, and two Na^{+} substitute into two M2 sites, as shown in Fig. 8b. The Al tetrahedra share edges with the Al octahedra. Owing to differences of ionic radius between Al^{3+} and host cations, the tetrahedra become expanded and the octahedra become compressed. Since the volume change of polyhedra is larger in the case of M-site substitution than in the case of T-site substitution, this structural modification results in shortening of the shared edges between octahedra and tetrahedra. The shortening of shared edges by substitution of Al^{3+} becomes stabilized in the olivine structure at high pressure from Pauling and Baur's third rule (Baur 1972). An excess charge of Al^{3+} in the M2-site could be compensated by Al^{3+} in the adjacent T-site. Excess charges of two Al^{3+} in the M1-site could be compensated by two Na^{+} in adjacent larger M2-sites. The Na substitution also compensates for the volume change in the host olivine. This is the reason why Al^{3+} substitution into octahedral sites increases significantly with pressure (Fig. 6). Positive correlation of pressure dependence of $D_{Al}^{ol/melt}$ is due to incorporation of Al^{3+} into the M-site of olivine.

The changes of mono- and tri-valent parabolic line on the Onuma diagram

Tri- and mono-valent cations show a large pressure dependence, in particular, $D_{Al}^{ol/melt}$ and $D_{Na}^{ol/melt}$ increase with increase in pressure because of the crystal chemistry of the olivine structure as discussed in the previous section. Partition coefficients of other trivalent cations (Cr, V, Sc and Y) decrease with increase in pressure, whereas, partition coefficients for monovalent cations increase with increasing pressure.

To examine the ionic radius at the peak position of the M-site on Onuma diagrams, parabolic lines were fitted using a strain energy model (Blundy and Wood 1994). The ionic radius at the peak position was calculated from partition coefficient for Al, V and Sc. The calculated peak position for the trivalent parabola is within the range of

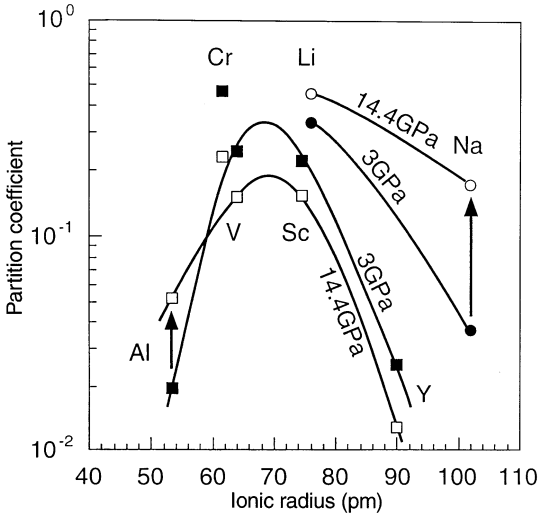

Fig. 9 The pressure dependence of mono- and tri-valent parabolas on PC-IR diagram between olivine and the coexisting melts. *Solid circle* KLB-22 (monovalent cations), *solid square* KLB-22 (trivalent cations), *open circle* KLB-43 (monovalent cations), *open square* KLB-43 (trivalent cations)

66.5 pm and 69.5 pm over the range of experimental pressure, i.e., the peak position is almost constant (Fig. 9). Therefore, the change of $D_{Al}^{ol/melt}$ or $D_{Na}^{ol/melt}$ with pressure is not due to the change of optimum ionic radius of the M-site.

The slope of the left-half side of the curve for trivalent cations and right-half side of the curve for monovalent cations becomes shallower with increase in pressure, although the slope of the right-half side of the curve for trivalent cations is unchanged (Fig. 9). Based on the crystal chemistry of olivine discussed in the previous section, substitution of a small cation such as Al^{3+} in the M site stabilizes the crystal structure at high pressures. Therefore, the pressure dependence of the parabolic curves on Onuma diagrams is interpreted to reflect that smaller trivalent cations substitute on the M-site, while such substitutions become more difficult for larger trivalent cations. Substitution of monovalent cations accompanies the substitution of small cations, and is required for electrostatic charge compensation and volume compensation. Accordingly the increase in partition coefficients for monovalent cations is accompanied by an increase of partition coefficients for small trivalent cations.

The changes of partition coefficient of divalent cations

Divalent cations substitute into the M site in olivine. Among the divalent cations observed, Ni, Co and Fe exhibit crystal field effects. Partition coefficients for these cations show strong pressure dependence in comparison with those for other divalent cations without crystal field effects (e.g. Mg, Mn and Ca) (Fig. 4). Plots of Ni, Co and Fe in Onuma diagrams obviously deviate from smooth parabolic curves for the M-site, especially at high pres-

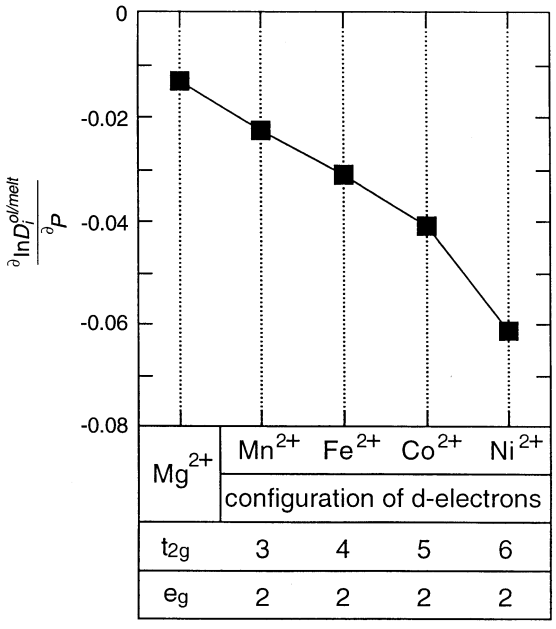

Fig. 10 $\partial \ln D_i^{ol/melt}/\partial P$ of Ni, Co, Fe, Mn and Mg

sures (Fig. 3). Figure 10 shows a comparison of pressure dependence, $(\partial \ln D_i^{ol/melt}/\partial P)$, of partition coefficients among Mg, Mn, Fe, Co and Ni calculated from Fig. 4. The partition coefficient of Ni has the largest pressure dependence among them. The degree of pressure dependence has the order Ni>Co>Fe.

From crystal field theory, the energy level of the d-orbital (e_g and t_{2g} orbital) of a cation is affected by the location of oxygen ligands (Burns 1972). The interaction among the orbitals and ligands is the most important factor for determining the stability of transition metals in the M-sites. The degree of pressure dependence among Ni, Co and Fe correlates to the number of d-electrons, in the t_{2g} orbitals of each cation (Fig. 10). The t_{2g} orbitals have their greatest electron density in a direction between the x-y-z axes.

The M–O distances of M-sites decrease up to the pressure at which olivine transforms to modified spinel (Hazen 1976; Kudoh and Takeuchi 1985). The distortion factors (Robinson et al. 1971) of M-sites in olivine increase with pressure, and the distortion results in a decrease of octahedral volume. The localized t_{2g} orbital of the transition metal ions is a stumbling block to the pressure induced compression of M-site octahedra. Therefore, M-site substitution of cations with strong crystal field effects under high pressure would destabilize the olivine structure in comparison with the substitution of cations without crystal field effects. Since the destabilization occurs by repulsive force between electrons of t_{2g} orbitals and coordinated oxygen, the cation with a larger number of t_{2g} electrons becomes more difficult to distribute in olivine at high pressure. The variation of pressure dependence of partition coefficients among divalent cations is attributed to the compression of the M-site polyhedra induced by pressure. Therefore, distribution of cations with strong crystal field effects is a good candidate for geobarometry at high pressures.

Conclusion

The following conclusions can be made regarding the systematics of cation partitioning between olivine and melt at high pressures:

(1) The partition coefficients of tri- and mono-valent cations show a large pressure dependence, both showing an increase in D with increase in pressure. This pressure dependence suggests that the partition coefficients are controlled by the substitution mechanism into the olivine crystal structure.
(2) Among mono- and tri-valent cations Na, Al and Cr are dominant species in mantle olivine. At low pressure a coupled substitution of $(Si^{4+}, Mg^{2+})\leftrightarrow(Al^{3+}, Cr^{3+})$ is dominant, whereas, at higher pressure the substitutions of $(Si^{4+}, Mg^{2+})\leftrightarrow(Al^{3+}, Al^{3+})$ and $(Mg^{2+}, Mg^{2+})\leftrightarrow(Na^{+}, Al^{3+})$ become dominant. The latter two substitution types occur in the ratio of 1:2. As a result, the amount of Al^{3+} in the T-site remains constant over the experimental conditions, and the Al^{3+} contents of M-sites increase significantly with pressure. The substitution of Al^{3+} reduces the cell volume of olivine, and such volume compression is favored at high pressures.
(3) The calculated peak position of trivalent parabola using a strain energy model is almost constant over the range of experimental pressures. Therefore, the change of partition coefficients for Al and Na with pressure is not due to the change of optimum ionic radius of the M-site in olivine. The pressure dependence of partition coefficients is interpreted such that smaller trivalent cations easily substitute into the M-site while it becomes more difficult for larger trivalent cations to substitute into the M-site by pressure induced compression of unit cell volume. The increase of partition coefficients for monovalent cations is accompanied by an increase of partition coefficients for small trivalent cations.
(4) The degree of pressure dependence among divalent cations correlates to the number of d-electrons in the t_{2g} orbital of each cation. Since destabilization occurs by repulsive force between electrons of t_{2g} orbitals and coordinated oxygen, the pressure dependence of the partition coefficient is attributed to the compression of the M-site polyhedra induced by pressure.

Acknowledgements The authors are grateful to Dr. S. Ozawa for permission to use his run charges. Critical reviews by Dr. M.J. Walter and an anonymous referee improved this manuscript very much. The authors are also grateful to Prof. M. Akaogi for editorial handling. This study was funded by the Monbu-sho and by the KagakuGijutsu-cho grants.

References

Abe Y (1993) Thermal evolution and chemical differentiation of the terrestrial magma ocean. Geophys Monogr. Am Geophys Union 74/IUGG 14:41–54

Agee CB (1993) Petrology of the mantle transition zone. Ann Rev Earth Planet Sci 29:19–41

Agee CB, Walker D (1990) Aluminum partitioning between olivine and ultrabasic silicate liquid to 6 GPa. Contrib Mineral Petrol 105:243–254

Ando A, Kamioka H, Terashima S, Itoh S (1989) 1988 values for GSJ rock reference samples, "Igneous rock series". Geochem J 23:143–148

Baur WH (1972) Computer-simulated crystal structures of observed and hypothetical Mg_2SiO_4 polymorphs of low and high density. Am Mineral 57:709–731

Beattie P (1994) Systematics and energetics of trace-element partitioning between olivine and silicate melts: implications for the nature of mineral/melt partitioning. Chem Geol 117:57–71

Benninghoven A, Rüdenauer FG, Werner HW (1986) Secondary ion mass spectrometry. Wiley, New York

Birle JD, Gibbs GV, Moore PB, Smith JV (1968) Crystal structures of natural olivines. Am Mineral 53:807–824

Blundy JD, Wood BJ (1994) Prediction of crystal-melt partition coefficients from elastic moduli. Nature 372:452–454

Burns RG (1970) Mineralogical applications of crystal field theory. Cambridge University Press, Cambridge

Colson RO, Mckay GA, Taylar LA (1988) Temperature and composition dependences of trace partitioning: olivine/melt and low-Ca pyroxene/melt. Geochim Cosmochim Acta 52:539–553

Hazen RM (1976) Effect of temperature and pressure on the crystal structure of forsterite. Am Mineral 61:1280–1293

Herzberg CT (1984) Chemical stratification in the silicate Earth. Earth Planet Sci Lett 67:249–260

Jurewicz AJG, Watson EB (1988) Cations in olivine, Part 1. Calcium partitioning and calcium-magnesium distribution between olivines and coexisting melts, with petrologic applications. Contrib Mineral Petrol 99:176:185

Kudoh Y, Takeuchi Y (1985) The crystal structure of forsterite Mg_2SiO_4 under high pressure up to 149 kb. Z Kristallogr 171:291–302

Matsui Y, Onuma N, Nagasawa H, Higuchi H, Banno S (1977) Crystal structure control in trace element partition between crystal and magma. Bull Soc Fr Mineral Cristallogr 100:315–324

Ohtani E (1984) Generation of komatiite magma and gravitational differentiation in the deep upper mantle. Earth Planet Sci Lett 67:261–272

Ohtani E, Kato T, Sawamoto H (1986) Melting of a model chondritic mantle to 20 GPa. Nature 322:352–353

Onuma N, Higuchi H, Wakita H, Nagasawa H (1968) Trace element partitioning between two pyroxenes and the host lava. Earth Planet Sci Lett 5:47–51

Ozawa S (1991) Trivalent cations in olivine and their implication to the upper mantle tectonics as inferred from the high pressure experiments. Doctoral thesis, Univ. of Tokyo

Robinson K, Gibbs GV, Ribbe PH (1971) Quadratic elongation: a quantitative measure of distortion in coordination polyhedra. Science 172:567–570

Scarfe CM, Takahashi E (1986) Melting of garnet peridotite to 13 GPa and the early history of the upper mantle. Nature 322:354–356

Shannon RD (1976) Revised effective ionic radii and systematic studies of interatomic distances in halides and chacogenides. Acta Crystallogr A32:751–767

Suzuki T, Akaogi M (1995) Element partitioning between olivine and silicate melt under high pressure. Phys Chem Minerals 22:411–418

Takahashi E (1978) Partitioning of Ni^{2+}, Co^{2+}, Fe^{2+}, Mn^{2+} and Mg^{2+} between olivine and silicate melts: compositional dependence of partition coefficient. Geochim Cosmochim Acta 42:1829–1844

Takahashi E (1986) Melting of a dry peridotite KLB-1 up to 14 GPa: implications on the origin of peridotitic upper mantle. J Geophys Res 91:9367–9382

Yurimoto H, Sueno S (1984) Anion and cation partitioning between olivine, plagioclase phenocrysts and the host magma: a new application of ion microprobe study. Geochem J 18:85–94

Yurimoto H, Yamashita A, Nishida N, Sueno S (1989) Quantitative SIMS analysis of GSJ rock reference samples. Geochem J 23:215–236

Yurimoto H, Sakaguchi I, Nishida N, Sueno S (1991) Determination of nickel in GSJ standard rock samples using secondary ion mass spectrometry. Geostandards Newsletter 15:155–159

Zhang J, Herzberg C (1994) Melting experiments on anhydrous peridotite KLB-1 from 5.0 to 22.5 GPa. J Geophys Res 99:17729–17742

Zhang J, Herzberg C (1996) Melting experiments on anhydrous peridotite. KLB-1: compositions of magmas in the upper mantle and transition zone. J Geophys Res 101:8271–8295